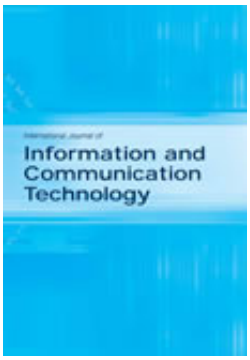

International Journal of Information and Communication Technology

ISSN online: 1741-8070 - ISSN print: 1466-6642
https://www.inderscience.com/ijict

Fault diagnosis model based on adaptive generalised morphological filtering and LLTSA-ELM

Jie Xiao, Jingtao Li, Chao Deng, Zhigang Luo, Huafeng Lin

DOI: 10.1504/IJICT.2023.10052207

Article History:

Received:	21 November 2019
Last revised:	15 January 2020
Accepted:	29 February 2020
Published online:	14 December 2022

Fault diagnosis model based on adaptive generalised morphological filtering and LLTSA-ELM

Jie Xiao and Jingtao Li*

Faculty of Information Engineering and Automation,
Kunming University of Science and Technology,
Kunming, 650500, China
Email: baibingyi1@sina.com
Email: 15127522495@163.com
*Corresponding author

Chao Deng, Zhigang Luo and Huafeng Lin

Electrical Engineering Co., Ltd. of China Railway 12th Bureau Group,
Tianjin, 300000, China
Email: 718321161@qq.com
Email: 1803237512@qq.com
Email: 454715164@qq.com

Abstract: It is difficult for a single feature to contain all the information needed to describe the running state of the equipment. Though multi-features can contain more information about running state, the redundancy between high-dimension features can easily reduce the accuracy of the classifier. Aimed at that, a fault diagnosis method for rolling bearings combining adaptive generalised morphological filter, linear local tangent space alignment and extreme learning machine (LLTSA-ELM) is proposed. Firstly, the rolling bearing vibration signals are filtered by an adaptive generalised morphological filter. Secondly, the multi-domain features are extracted from filtered signal to construct high-dimensional features set of bearing. Thirdly, the dimension of high-dimensional features is reduced by maximum likelihood estimation (MLE) and LLTSA. Finally, the bearing condition monitoring model based on ELM is constructed by the reduced dimension features, and then is used to analyse and diagnose the running state of bearing. Experiments show that this method can effectively filter noise, reduce the redundancy caused by high-dimensional features, and improve the recognition accuracy of the running state of bearings.

Keywords: adaptive generalised morphological filter; linear local tangent space alignment; LLTSA; dimension reduction; extreme learning machine; ELM; fault diagnosis.

Reference to this paper should be made as follows: Xiao, J., Li, J., Deng, C., Luo, Z. and Lin, H. (2023) 'Fault diagnosis model based on adaptive generalised morphological filtering and LLTSA-ELM', *Int. J. Information and Communication Technology*, Vol. 22, No. 1, pp.1–14.

Biographical notes: Jie Xiao received his Bachelor's degree from Donghua University in 2017 and Master's degree from Kunming University of Technology in 2020. His main research interests are fault diagnosis and machine learning.

Jingtao Li is an Associate Professor at the Kunming University of Technology and his main research interests are big data analysis and high-density computing.

Chao Deng mainly focuses on traffic signal and automatic control and is currently affiliated with Electrical Engineering Co., Ltd. of China Railway 12th Bureau Group.

Zhigang Luo graduated from Electronic Information Engineering of Jianghan University and is currently affiliated with Electrical Engineering Co., Ltd. of China Railway 12th Bureau Group.

Huafeng Lin is an Assistant Engineer. He graduated from East China Jiaotong University, majoring in transportation equipment information.

1 Introduction

With the development of intelligent manufacturing, equipment tends to be fine and the working environment is more complicated, that greatly increases the difficulty of mechanical equipment fault diagnosis. How to effectively diagnose and monitor the fault of complex equipment has become a research focus (Rai and Upadhyay, 2016; Fengtao and Liu, 2018; Cerrada et al., 2018).

Signal denoising is the major issue to non-stationary signal pre-processing. The regular methods are empirical mode decomposition (EMD), local mean decomposition (LMD) and wavelet decomposition (WD). However, the parameters of above methods depend too much on human experience and the high calculation complexity can damage the real-time performance of online fault diagnosis. In recent years, morphological filter has been widely used in nonlinear signal processing (Lv and Yu, 2018). Huang et al. (2018) employed generalised morphological filter and MRSVD for extracting fundamental frequency component of rolling bearing faults. In order to solve the problems of morphological structure element selection and the inherent statistical deviation, Qian et al. (2017) used particle swarm optimisation algorithm to optimise the generalised morphological filter. Jiang et al. (2011) used gradient method to carry out adaptive weighting processing for generalised morphological filter, and realised its adaptive filter. Jiang et al. (2018) used LMS algorithm to process the weight coefficients of the generalised morphological filter which is effectively to filter the bearing vibration signal noise.

Feature extraction is one of the key part in equipment condition monitoring and fault diagnosis. It has become one of the research trends to construct high-dimensional features extracted from equipment status information to diagnose equipment fault. Xu et al. (2016) combined ensemble empirical mode decomposition (EEMD), principal component analysis (PCA) and Gath-Geva (GG) method to reduce the dimension of the fault diagnosis model and increase the fault diagnosis accuracy of the model. Xu et al. (2012) used PCA to reduce the dimension of multi-sensor data, and use RBF to diagnose fault of coal mine equipment. Luo et al. (2007) used linear discriminant analysis (LDA) to reduce the dimension of high-dimensional features constructed by genetic coding, and realised fault identification through multi-class support vector machines (SVMs).

However, above algorithms disagree with nonlinear problems. As a good nonlinear dimension reduction method in manifold learning, local tangent space alignment (LTSA), can effectively extract the low-dimensional manifold structure of high-dimensional features. But it is greatly affected by the selection of neighbouring points. For data with uneven distribution of features and large curvature, it is difficult to obtain better results, while linear local tangent space alignment (LLTSA) overcomes the shortcomings of LTSA and effectively extracts the essential features of high-dimensional features.

In recent years, extreme learning machine (ELM) has been widely used. Compared with neural network (NN), SVM and ensemble learning (EL), ELM has the advantages of fewer parameters and faster training speed. It is more suitable for real-time monitoring and diagnosis of equipment.

Overall, a fault diagnosis method based on adaptive generalised morphological filter and LLTSA-ELM is proposed in this paper. Firstly, the vibration signal is filtered by adaptive generalised morphological filter. Then, the high-dimensional features set are constructed by extracting the time-domain features, frequency-domain features, wavelet entropy and approximate entropy from the de-noised signal. Finally, the dimension of multi-features is reduced by using maximum likelihood estimation (MLE) and LLTSA. The fault diagnosis model (Huang and Li, 2015) is established by ELM to identify the equipment status. The experimental results show that this method can effectively filter noise, reduce the redundancy between high-dimensional features and improve the recognition accuracy of classifiers.

2 Adaptive generalised morphological filter

Let $f(n)$, $n = 0, 1, 2, \ldots, N-1$ be the original discrete input signal, $g(m)$, $m = 0, 1, 2, \ldots, M-1$ be the structural element, and $N \geq M$. The four basic operators, erosion, dilation, opening, closing can be defined as equations (1)–(4):

$$(f \Theta g)(n) = \min\left[x(n+m) - g(m)\right] \tag{1}$$

$$(f \oplus g)(n) = \max\left[x(n-m) + g(m)\right] \tag{2}$$

$$(f \circ g)(n) = (f \Theta g) \oplus g \tag{3}$$

$$(f \cdot g)(n) = (x \oplus g) \Theta g \tag{4}$$

The open operation is applying corrosion before dilation, which can eliminate the spick noise, and the closed operation is applying dilation before erosion, which can fill the small voids and fill the broken marks in the waveform. On the basis of traditional morphology, Yu et al. (2018) proposed an improved morphological filter. There are two structural elements with different sizes g_1, g_2, the improved morphological filter are defined as follows:

$$GOC(n) = \left(f \cdot g_1 \circ g_2\right)(n) \tag{5}$$

$$GCO(n) = \left(f \circ g_1 \cdot g_2\right)(n) \tag{6}$$

$$F(n) = (GOC + GCO)/2 \tag{7}$$

Although above process can effectively eliminate noise, it has strong dependence and randomness on structural elements. Aimed at that problems, Jiang et al. (2018) proposed an adaptive generalised morphological difference filter to de-noising the signal adaptively by using a weighted coefficients a. Let the input signal be $x(n)$, the ideal signal be $s(n)$, the output signal can be defined as follows:

$$y(n) = a_1(n)y_1(n) + a_2(n)y_2(n) \tag{8}$$

The error is:

$$e(n) = s(n) - y(n) \tag{9}$$

The mean square error is:

$$E[e^2] = E\left[|s(n) - y(n)|^2\right] \tag{10}$$

The least mean square (LMS) method is used to adjust the value of weighting coefficients; the square of samples error $e^2(n)$ is used to estimate the mean square error; the partial derivative of weighting coefficients is obtained. The steepest descent method is used to optimise the weighting coefficients, then:

$$a_i(n+1) = a_i(n) + 2\mu y_i(n)e(n) \tag{11}$$

where $i = 1, 2$, μ is the controlling convergence speed parameters.

3 Feature extraction and dimension reduction

In this paper, 29 time-domain and frequency-domain features, as well as wavelet entropy and approximate entropy, are extracted to construct a high-dimensional dataset to describe the operation status of the equipment. MLE is used to find the low-dimensional intrinsic of high-dimensional features and LLTSA is used to reduce the redundancy between high-dimensional feature vectors.

3.1 Multi-domain features, approximate entropy and wavelet entropy

In the time-domain, 16 features such as mean, root mean square value, root square amplitude, absolute mean value, skewness, kurtosis, variance, maximum value, minimum value, peak value, kurtosis index, peak value index, skewness index, margin index, waveform index and pulse index were selected. In the frequency-domain, 13 features such as mean frequency, standard deviation, 7 spectral dispersion, 2 main frequency position, root mean square frequency and frequency centre were selected (Xiao et al., 2015), as shown in Table 1.

Approximate entropy (*ApEn*) can describe the complexity and irregularity of time series, and it has strong anti-noise interference ability. It is widely used in the field of mechanical equipment diagnosis. We proceed as follows:

a Give an one-dimensional time series $\{u(i), i = 0, 1, \ldots, N\}$, after expansion, reconstructed as a m-dimensional vector $X(i)$ as:

$$X(i) = [u(i), u(i+1), \ldots, u(i+m-1)] \tag{12}$$

where $i = 1 \sim N - m + 1$.

b Compute the distance between different vectors, X_i, X_j by:

$$d\left[X(i), X(j)\right] = \max\left|u(i+k) - u(j+k)\right| \tag{13}$$

where $k = 0, 1, \ldots, m - 1$.

c Setting threshold r ($r > 0$), let A_i be the number of $d[X(i), X(j)]$ within r, define the function:

$$C_m^i(r) = A_i / N - m + 1 \tag{14}$$

d Define the average of the natural logarithms of the function $C_m^i(r)$ as:

$$j^m(r) = \frac{1}{N-m+1} \sum_{i=1}^{N-m+1} \ln C_i^m(r) \tag{15}$$

e Let $m = m + 1$, repeat a–d computing $\Phi^{m+1}(r)$, $ApEn(m, r, N)$ is defined as:

$$ApEn(m, r, N) = \Phi^m(r) - \Phi^{m+1}(r) \tag{16}$$

Table 1 Mathematical expression of frequency domain features

No.	*Feature expression*
1	$f_1 = \frac{1}{K}\sum_{k=1}^{K} s(k)$
2	$f_2 = \frac{1}{K-1}\sum_{k=1}^{K} (s(k) - f_1)^2$
3	$f_3 = \frac{\sum_{k=1}^{K} (s(k) - f_1)^3}{K(\sqrt{f_2})^3}$
4	$f_4 = \frac{\sum_{k=1}^{K} (s(k) - f_1)^4}{K(f_2)^4}$
5	$f_5 = \frac{\sum_{k=1}^{K} s(k) f_k}{\sum_{k=1}^{K} s(k)}$
6	$f_6 = \sqrt{\frac{\sum_{k=1}^{K} s(k) \times (f_k - f_5)^2}{K}}$
7	$f_7 = \sqrt{\frac{\sum_{k=1}^{K} s(k) f_k^2}{\sum_{k=1}^{K} s(k)}}$
8	$f_8 = \sqrt{\frac{\sum_{k=1}^{K} s(k) f_k^4}{\sum_{k=1}^{K} s(k) f_k^2}}$

Table 1 Mathematical expression of frequency domain features (continued)

No.	*Feature expression*
9	$f_9 = \dfrac{\sum_{k=1}^{K} s(k) f_k^2}{\sqrt{\sum_{k=1}^{K} s(k) \sum_{k=1}^{K} s(k) f_k^2}}$
10	$f_{10} = \dfrac{f_6}{f_5}$
11	$f_{11} = \dfrac{\sum_{k=1}^{K} (f_k - f_5)^3 s(k)}{K(f_6)^3}$
12	$f_{12} = \dfrac{\sum_{k=1}^{K} (f_k - f_5)^4 s(k)}{K(f_6)^4}$
13	$f_{13} = \dfrac{\sum_{k=1}^{K} (f_k - f_5)^{1/2} s(k)}{K(f_6)^{1/2}}$

In this paper, set $r = 0.25$, $m = 2$, compute the *ApEn* of original signal.

Wavelet entropy reflects the sparsity and orderliness of the signal by computing the entropy value of the probability distribution sequence after WD. It has high sensitivity to abnormal signal and can monitor the abnormal state of the system in time and effectively. Give a continuous signal $f(t)$, the wavelet transform of $f(t)$ is defined as:

$$W_f(a, \tau; \psi) = \int f(t) \psi_{a,\tau}(t) dt \tag{17}$$

Where a is the scale parameter and $a > 0$; τ is the translation parameter; $\psi_{(a,\tau)}(t)$ is generated by dilation and translation of a wavelet $\psi(t)$: $\psi_{a,\tau}(t) = a^{-1/2} \psi\left(\dfrac{t-\tau}{a}\right)$.

Divided time-frequency domain of signal transformed by wavelet transform into N time-frequency regions, assume E_1, E_2, …, E_n are the energy component of the signal in each subspace in the same time period, and the total energy of the signal in that time period is defined as: $E = \sum_{i=1}^{N} E(i = 1, 2, \ldots, N)$. Assume $p_i = E_i / E$, the wavelet entropy can be defined as

$$W_E = -\sum_{i=1}^{n} p_n \ln(p_n) \tag{18}$$

In this paper, the wavelet basis is DB6 and the decomposition level is 6. Seven wavelet entropy values are obtained.

3.2 Estimate the intrinsic dimension by MLE

Choosing the appropriate eigenvalue dimension is very important to achieve the balance between noise elimination and effective dimension reduction. The MLE method

establishes the likelihood function of Euclidean distance of adjacent points (Ma et al., 2015) based on the existing sample data, and estimates the unknown parameters by taking the parameters under which the likelihood function reaches its maximum value.

Given a dataset with N samples $X = \{x_1, x_2, \ldots, x_N\}$, the basic ideal is to fix a point x, assume $f(x) \approx c$ (c is a constant) in a small sphere $S_x(R)$ of radius R around x_i, and treat that random process as a homogeneous Poisson process in $S_x(R)$. $N(t, x)$ is the number within distance t from x, the function is defined as:

$$N(t, x) = \sum I\{x \in S_x(t)\} \tag{19}$$

Let the unit sphere volume of $S_x(R)$ be $V(m)$, the log-likelihood of the observed process $N(t)$ can be written as:

$$L(m, \theta) = \int_0^R \lg \lambda(t) dN(t) - \int_0^R \lambda(t) dt \tag{20}$$

where $\lambda(t) = f(x)V(m)dt^{m-1}$.

Compute partial derivatives of the parameters d, θ respectively and let them are equal to 0, give the local optimal dimension m:

$$d\hat{m}_R(x) = \left[\frac{1}{N(R, x)} \sum_{j=1}^{N(R,x)} \lg \frac{R}{T_j(x)} \right]^{-1} \tag{21}$$

Use the number of neighbours k replace the radius of the sphere R, then equation (21) becomes:

$$\hat{m}_K(x) = \left[\frac{1}{K-1} \sum_{j=1}^{K-1} \lg \frac{TK(x_i)}{T_j(x)} \right]^{-1} \tag{22}$$

Then get the global intrinsic dimension:

$$\hat{d}_k = \sum_{i=1}^{N} \hat{m}_k(x_i) \tag{23}$$

3.3 LLTSA algorithm

LLTSA combines traditional dimension reduction algorithms PCA and LTSA. It uses tangent coordinates to express the set structure of local neighbourhoods, and then arranges these tangent plane information in low-dimensional space to express global coordinates. Its main idea is to find an external projection matrix A to transform the dataset in high-dimensional space into low-dimensional space and compute its low-dimensional expression.

Assuming the dataset is $X = [x_1, \ldots, x_N]$ in R^m, the algorithm steps of LLTSA can be defined as follows:

a Project the dataset X into PCA subspace, the projection matrix is denoted as A_{pca}. In order to describe conveniently, the data feature set is still expressed as X in following steps.

b For each x_i, $i = 1, 2, \ldots, N$, its k nearest neighbours are searched and denote it by a matrix $X_i = [x_{i_1}, \ldots, x_{i_k}]$.

c In order to save the local structure of each X_i, compute V_i which is constructed by the d right singular vectors of $X_i H_k$ corresponding to the maximum singular value of d. Set $W_i = H_k(I - V_i V_i^T), i = 1, \ldots, N,$ where $H_k = I - e_e^T / k$ denote the centralised matrix.

d Compute the alignment matrix B by:

$$B(I_i, I_i) \leftarrow B(I_i, I_i) + W_i W_i^T, i = 1, 2, \ldots, N \tag{24}$$

Initialisation $B = 0$, where $I_i = \{i_1, \ldots, i_k\}$ denote the indices set for k nearest neighbours of each x_i.

e Compute the transformation matrix. Solve the following generalised eigenvalue problems:

$$XH_N BH_N X^T \alpha = \lambda XH_N X^T \alpha \tag{25}$$

Then we get the eigenvalue $\lambda_1 < \lambda_2 < \ldots < \lambda_d$, and the eigenvectors corresponding to each eigenvalues are $\alpha_1 < \alpha_2 < \ldots < \alpha_d$, and we get $A_{LLTSA} = (\alpha_1, \alpha_2, \ldots, \alpha_d)$, so the transformation matrix is denoted as follows:

$$A = A_{pca} A_{LLTSA}, \text{ and } X \to Y = A^T XH_N \tag{26}$$

4 ELM model

ELM is a learning algorithm for single-hidden layer feed-forward networks (SLFNs). Given the training set as $S = \{(X_i, t_i) | X_t \in R^n, t_i \in R^m, i = 1, \ldots, N\}$, where X_i is the input and t_i is the target vector. Set the number of hidden layer unit as $\tilde{N}$, the weight matrix between input layer and hidden layer as $W = (w_{ij})_{\tilde{N} \times n}$, hidden layer threshold matrix as $b = (b_1, b_2, \ldots, b_{\tilde{N}})$, the activation function as $g(x)$, then the ELM model can be formulated as:

$$\sum_{i=1}^{\tilde{N}} g(w_i \cdot x_i + b_i)\beta_i = t_j, \ j = 1, 2, \ldots, N \tag{27}$$

To make it be more clear, equation (27) can be written in a more compact format by using matrix form as:

$$H\beta = T \tag{28}$$

ELM algorithm selects weights w_i and b_i randomly, and determines the output weights β by finding the least square solution of equation (28). By computing $\beta = H^+T$, where H^+ is the Moore-Penrose generalise inverse of H, we get the output weights β.

5 Bearing condition monitoring method based on adaptive generalised morphological filter and LLTSA-ELM

In this paper, a new bearing condition monitoring method combining adaptive generalised morphological filtering and LLTSA-ELM is proposed. Firstly, the bearing vibration signal is filtered by adaptive generalised morphological filter, and the noise components in the signal are filtered. Then, the multi-features of the filtered signal are extracted, and high-dimensional features of the signal is reduced by MLE and LLTSA. Finally, the bearing condition monitoring model is constructed by using the reduced features. The step by step can be denoted as follows:

1 The bearing vibration signal is filtered by adaptive generalised morphological filter to remove the noise components in the signal.

2 Extract the features of time-domain, frequency-domain, wavelet entropy and approximate entropy in denoising signals under different operating conditions, and construct the multi-features set.

3 The intrinsic dimension of bearing high-dimensional feature set is estimated by MLE.

4 According to the intrinsic dimension, the dimension of multi-features set is reduced into intrinsic dimension by LLTSA.

5 Based on the features after dimension reduction, the ELM bearing condition monitoring model is constructed, then use it to analyse and monitor the bearing condition.

6 Experiments

6.1 Experiments platform

The experimental data are from the bearing dataset of Kat Data Center, Padborn University, Germany (Kumar and Kumar, 2016). Rolling bearings with typical damage characteristics are generated in the accelerated lifetime test rig and the structure of the platform is shown in Figure 1. The main components are

1 drive motor

2 housing

3 adjusting nut

4 spring package.

The signals of the platform are the vibration signals collected by the acceleration sensor. The selected bearing data are the natural damage data collected by accelerated lifetime test equipment, including normal, inner ring fault and outer race fault. There are no types of rolling element fault found in the experiment, so the identification of rolling element fault type is not included in this experiment. The main specific information about test bearing is as shown as Table 2. The shaft rotational speed is 1,790 rpm, so the standard

fundamental frequency of out race fault and inner race are 104.56 Hz, 57.94 Hz respectively.

Figure 1 Experimental platform (see online version for colours)

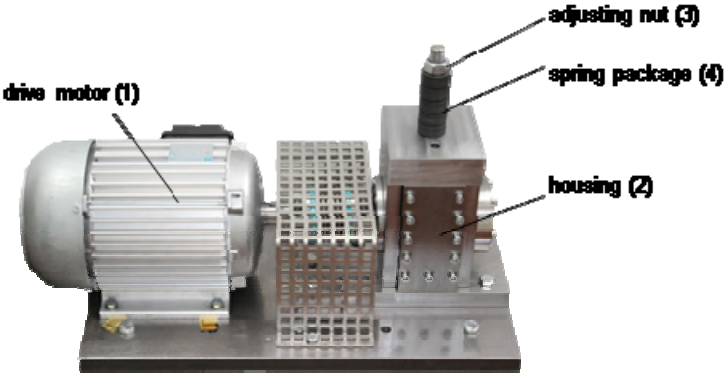

Table 2 specific information about test bearing

Bearing model	*Rolling element diameter*	*Pitch circle diameter*	*Number of rolling elements*	*Tapered contact angle*
6203	7.94 mm	39.04 mm	9 pc.	0°

6.2 Experimental results

The experimental samples include 100 samples of normal state, 100 samples of inner race fault state and 100 samples of outer race fault state, each of which has 10,240 multi-domain features. Each state is randomly divided into training set of 66 and test set of 34, totalling training set of 198 samples and test set of 102 samples.

Firstly, the time-domain waveform of the signal after adding the Gauss white noise with SNR of –1 is shown as Figure 2. The vibration signal is filtered by adaptive generalised morphological filtering to remove the noise of the signal which are independent of the state information. Figure 3 show the envelope spectrum without filter, and Figure 4 show the envelope spectrum after adaptive generalised morphological filter. By comparing the two graphs, it can be seen that the envelope image after adaptive generalised morphological filter has less noise. The fundamental frequency of the fault is more obvious.

Then, extract multi-features from normal state, outer race fault state and inner race fault state respectively. The 37-dimensional features of 10,240 sampling points in time-domain, frequency-domain, wavelet entropy and approximate entropy are taken as the feature vectors of a sample. The specific parameters of the features have been described in Subsection 3.1. 100 samples of each type are constructed and we have 300 * 37 samples set. And the intrinsic dimension of sample sets is computed by MLE. The result is three-dimension. Then the high-dimension features of the sample set are reduced into three-dimension by LLTSA. A new sample set of 300 * 3 is obtained.

Figure 2 Signal time domain diagram with gauss white noise (see online version for colours)

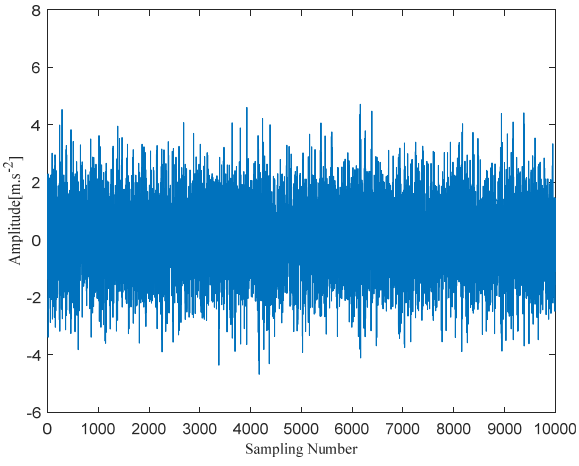

Finally, the new sample set of 300 * 3 is divided randomly into training set of 198 samples and test set of 102 samples. The ELM fault diagnosis model and SVM model are trained by the training set and then recognised by test set. Divide training set and test set ten times, and the diagnosis results are shown in Table 3.

In order to determine the effectiveness of the method in more complex situation, Gaussian white noise with 1 db is added to the original signal. Repeat the above experiments, the recognition rate of ELM model before dimension reduction is shown in Figure 5, the classification result of the test set is 51.96%. The recognition rate of ELM model after dimension reduction by LLTSA is shown in Figure 6, the classification result of the test set is 85.29%. The results show that LLTSA can effectively reduce the information redundancy between high-dimensional features and improve the recognition accuracy of classifiers. And the recognition rate of ELM bearing fault diagnosis model is generally higher than that of SVM.

Figure 3 Envelope spectrum before filter (see online version for colours)

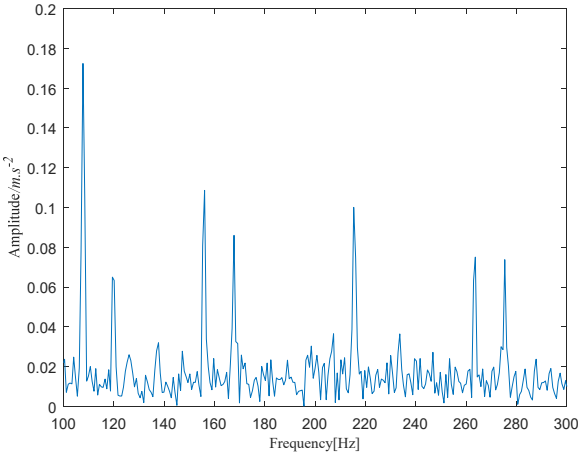

Figure 4 Envelope spectrum after filter (see online version for colours)

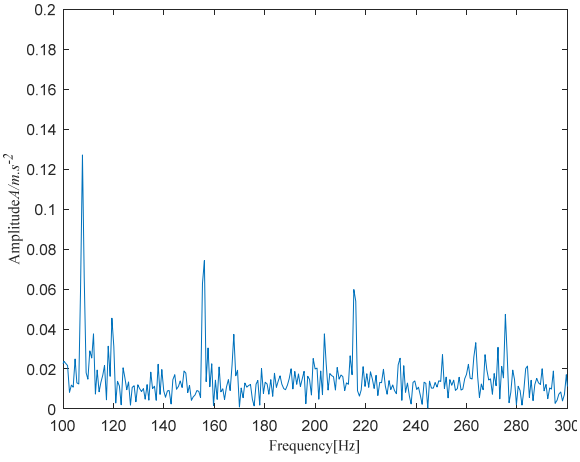

Figure 5 Classification results of the method based on ELM before dimension reduction (see online version for colours)

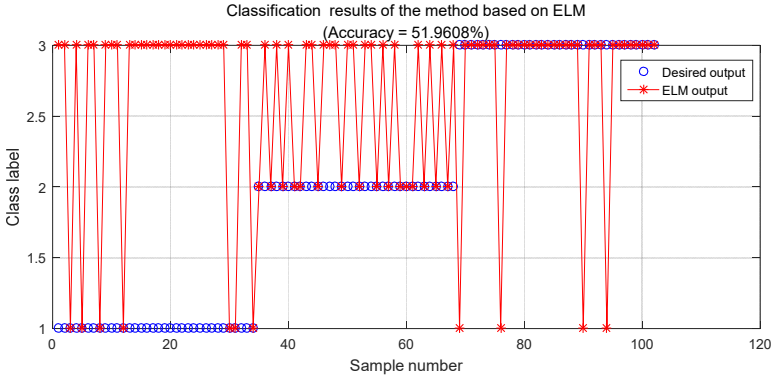

Figure 6 Classification results of the method based on LLTSA after dimension reduction by LLTSA (see online version for colours)

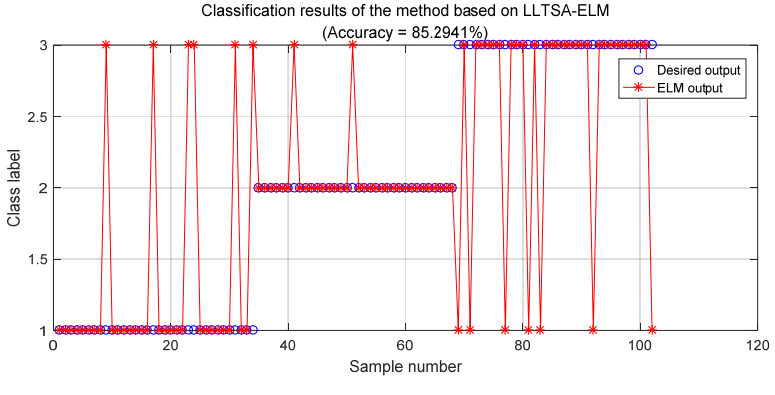

Table 3 Recognition results after multiple partitions of training sets and test sets

No.	*Before descending dimension, the accuracy of SVM (%)*	*Before descending dimension, the accuracy of ELM (%)*	*After descending dimension, the accuracy of SVM (%)*	*After descending dimension, the accuracy of ELM (%)*
1	34.31	96.08	93.14	100.00
2	35.29	80.39	66.67	85.29
3	41.18	91.18	92.16	98.04
4	34.31	66.67	74.51	90.20
5	34.31	100.00	92.16	98.04
6	34.31	94.12	91.18	99.02
7	33.33	86.27	94.12	99.02
8	33.33	67.65	92.16	98.04
9	34.31	72.55	96.08	99.02
10	36.27	72.55	91.18	99.02

7 Conclusions

1 This method that combined adaptive generalised morphological filter and LLTSA-ELM can effectively filter the noise components in the signal, reduce the information redundancy between high-dimensional feature vectors, and improve the classification accuracy of fault diagnosis model effectively.

2 The features selected in this paper are time-domain, frequency- domain and entropy value, which can denote the running state characteristics of bearing comprehensively. However, with the complexity of industrial system and working conditions, how to select appropriate features to describe the running state of equipment in different situations is becoming more and more complex. It is the direction of future research.

Acknowledgements

This work was finally supported by National Natural Science Foundation of China (No. 61663017) and Key Projects of Yunnan Science and Technology Plan (No. 2017FA027).

References

Cerrada, M., Sánchez, R-V. et al. (2018) 'A review on data-driven fault severity assessment in rolling bearings', *Mechanical Systems and Signal Processing*, Vol. 99, pp.169–196.

Chen, B., Shen, B., Chen, F. et al. (2019) 'Fault diagnosis method based on integration of RSSD and wavelet transform to rolling bearing', *Measurement*, Vol. 131, pp.400–411.

Fengtao, W. and Liu, C. (2018) 'A review of current condition monitoring and fault diagnosis methods for slewing bearings', *Innovative Techniques and Applications of Modelling, Identification and Control*, Vol. 467, pp.53–62.

Huang, G.J., Fan, Y.G., Feng, Z. et al. (2018) 'Research on fault diagnosis method based on generalized morphological filter and MRSVD', *Computer Engineering and Applications*, Vol. 54, No. 3, pp.217–221.

Huang, S. and Li, C. (2015) 'Distributed extreme learning machine for nonlinear learning over a network', *Entropy*, Vol. 17, No. 2, pp.818–840.

Jiang, Z., Deng, A.D., Cai, B.H. (2011) 'Application of an adaptive generalized morphological filter based on the gradient method in rubbing acoustic emission signal de-noise', *Proceedings of the Chinese Society for Electrical Engineering*, Vol. 31, No. 8, pp.87–92.

Jiang, Z., Deng, A.D., Cai, B.H. et al. (2018) 'Feature extraction method of ITD and adaptive generalized morphological filtering', *Transducer and Microsystem Technologies*, Vol. 37, No. 6, pp.36–39.

Kumar, A. and Kumar, R. (2016) 'Manifold learning using linear local tangent space alignment (LLTSA) algorithm for noise removal in wavelet filtered vibration signal', *Journal of Nondestructive Evaluation*, Vol. 35, No. 3, p.50.

Luo, G.Q., Song, W.Y. and Ma, X.F. (2007) 'An effective linear discriminant analysis (LDA) method based on genetic programming (GP) for extracting features in fault diagnosis', *Journal of Northwestern Polytechnical University*, Vol. 25, No. 3, pp.363–367.

Lv, J. and Yu, J. (2018) 'Average combination difference morphological filters for fault feature extraction of bearing', *Mechanical Systems and Signal Processing*, Vol. 100, pp.827–845.

Ma, J.H., Tang, B.P. and Song, T. (2015) 'Phase space reconstruction method for vibration signal's noise reduction based on adaptive intrinsic dimension estimation manifold learning', *Journal of Vibration and Shock*, Vol. 34, No. 11, pp.29–34.

Qian, L., Kang, M., Fu, X.Q. et al. (2017) 'Application of adaptive morphology in bearing fault diagnosis based on VMD', *Journal of Vibration and Shock*, Vol. 36, No. 3, pp.227–233.

Rai, A. and Upadhyay, S.H. (2016) 'A review on signal processing techniques utilized in the fault diagnosis of rolling element bearings', *Tribology International*, Vol. 96, pp.289–306.

Xiao, S.G., Ma, S.H., Song, M.M. et al. (2015) 'Performance degradation indicator extraction method of rolling bearings based on the EEMD and PCA', *Journal of Southern Yangtze University (Natural Science Edition)*, Vol. 14, No. 5, pp.572–579.

Xu, F., Fang, Y.J. and Zhang, R. (2016) 'PCA-GG rolling bearing clustering fault diagnosis based on EEMD fuzzy entropy', *Computer Integrated Manufacturing Systems*, Vol. 22, No. 11, pp.2631–2642.

Xu, G.Y., Jiang, H.S., Li, H. et al. (2012) 'Fault diagnosis of bearing based on WSN and data fusion algorithm of PCA-RBF', *Journal of China University of Mining & Technology*, Vol. 41, No. 6, pp.964–970.

Yan, X. and Jia, M. (2016) 'Parameter optimized combination morphological filter-hat transform and its application in fault diagnosis of wind turbine', *Journal of Mechanical Engineering*, No. 13, p.14.

Yu, J.B., Lv, J.X., Cheng, H. et al. (2018) 'Fault diagnosis for rolling bearing based on ITD and improved morphological filter', *Journal of Beijing University of Aeronautics and Astronautics*, Vol. 44, No. 2, pp.241–249.